*Circ J* 2005; **69:** 1003–1006

# Coexistence of the Permanent Form of Junctional Reciprocating Tachycardia and Atrial Tachycardia

Takashi Noda, MD; Wataru Shimizu, MD; Kazuhiro Suyama, MD; Takeshi Tobiume, MD; Kazuhiro Satomi, MD; Takashi Kurita, MD; Naohiko Aihara, MD; Shiro Kamakura, MD

This case report describes a patient with the permanent form of junctional reciprocating tachycardia coexisting with atrial tachycardia. A detailed electrophysiological study established the diagnosis, and radiofrequency catheter ablation abolished both arrythmias. (*Circ J* 2005; **69:** 1003–1006)

**Key Words:** Atrial tachycardia; Catheter ablation; Permanent form of junctional reciprocating tachycardia (PJRT); Supraventricular tachycardia

The permanent form of junctional reciprocating tachycardia (PJRT) is a rare supraventricular tachycardia in which retrograde ventriculoatrial (VA) conduction occurs with a decremental property[1,2] PJRT is frequently incessant and occasionally tachycardia-induced cardiomyopathy develops. The electrocardiographic feature of PJRT is a narrow QRS tachycardia with a long RP' interval. However, atypical forms of atrioventricular (AV) node reentry tachycardia (AVNRT) and atrial tachycardia (AT) show similar electrocardiographic findings. Therefore, a detailed electrophysiological study (EPS) must be done to establish the diagnosis. We describe a patient with coexisting PJRT and AT.

## Case Report

A 31-year-old woman was referred to hospital for recurrent episodes of palpitation, the first attack of which had occurred 1 year ago and since then, the frequency had increased 2 or 3 times a day. She was treated with verapamil, but it did not completely suppress the attacks. A 12-lead electrocardiogram during sinus rhythm did not show a delta wave, but a narrow QRS tachycardia characterized by a negative P wave in leads II, III, and aVF with a long RP' interval was documented during a palpitation attack. An extensive work up, including echocardiographic study, did not reveal any structural heart disease.

She underwent an EPS after giving written informed consent. Two standard quadripolar electrode catheters were positioned at the high lateral right atrium (HRA) and right ventricular apex (RVA). An octapolar electrode catheter was positioned at the His bundle and a 2.5Fr 16-electrode catheter was positioned in the coronary sinus. At baseline, extrastimulation from the RVA induced slow VA conduction with a decremental property, and the narrow QRS tachycardia was not induced by any pacing protocols. However, after isoproterenol infusion, a clinically documented narrow QRS tachycardia (Tachycardia 1) was induced by a single extrastimulus from the RVA (Fig 1A). Intracardiac tracing during Tachycardia 1 revealed that the earliest atrial activation was recorded near the coronary sinus ostium and the RVA–HRA interval was 200 ms. A single ventricular extrastimulus, which was introduced from the RVA when the His bundle was refractory, delayed the subsequent atrial activation ("postexcitation" phenomenon) (Fig 2). A retrograde VA conduction time (St (RV)-A2) curve was obtained after a single ventricular extrastimulus during Tachycardia 1 (Fig 3). Shortening of the coupling intervals of the extrastimulus (RV-St (RV)) resulted in increases in St (RV)-A2, indicating that the retrograde VA conduction during Tachycardia 1 had a decremental property. Based on these observations, Tachycardia 1 was diagnosed as PJRT and radiofrequency catheter ablation (RFCA) performed at the earliest atrial activation site near the coronary sinus ostium was able to terminate it. However, the other narrow QRS tachycardia with a long RP' interval (Tachycardia 2; Fig 1B) was induced by a single extrastimulus from RVA with isoproterenol infusion and the RVA–HRA interval was 208 ms. Tachycardia 2 was unstable, and subsequently changed to another narrow QRS tachycardia (Tachycardia 3; Fig 1C). The RVA–HRA interval during Tachycardia 3 was 108 ms and shorter than that of Tachycardia 1 or 2. A single ventricular extrastimulus could not affect the atrial activation sequence during Tachycardia 3 when the His bundle was refractory. Moreover, burst pacing from the RVA demonstrated AV dissociation without affecting the cycle length of Tachycardia 3 (Fig 4), suggesting that Tachycardia 3 was AT. Detailed endocardial mapping during Tachycardia 3 showed that the earliest site of atrial activation was in the posterolateral right atrium near the tricuspid annulus. A single burst of RF energy immediately changed Tachycardia 3 to Tachycardia 2, which then terminated spontaneously. However, there was residual VA conduction with the same atrial activation sequence as Tachycardia 2, so we performed RFCA at the earliest site via retrograde VA conduction in the midseptum of the right atrium (between the His bundle and coronary sinus ostium) to eliminated it. Finally, there was

*(Received January 13, 2005; revised manuscript received May 18, 2005; accepted May 25, 2005)*
*Division of Cardiology, Department of Internal Medicine, National Cardiovascular Center, Suita, Japan*
Mailing address: Wataru Shimizu, MD, Division of Cardiology, Department of Internal Medicine, National Cardiovascular Center, 5-7-1 Fujishiro-dai, Suita 565-8565, Japan. E-mail: wshimizu@hsp.ncvc.go.jp

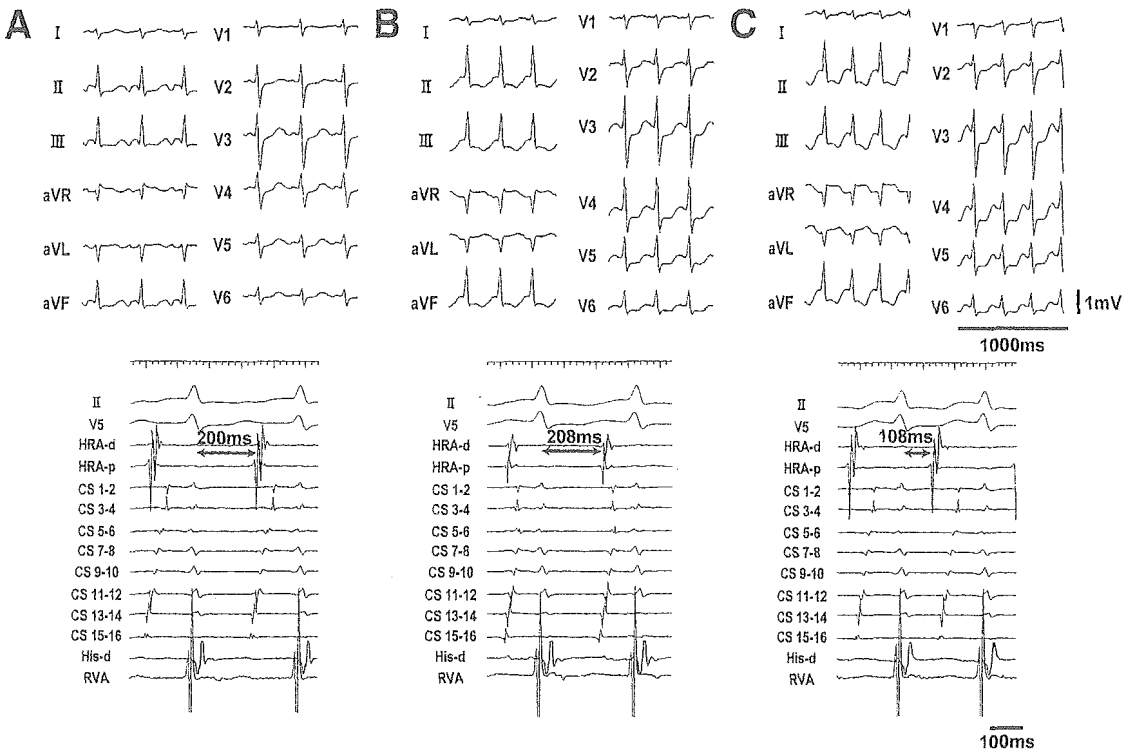


Fig 1. Twelve-lead electrocardiograms and intracardiac tracings during Tachycardia 1 (A), Tachycardia 2 (B), and Tachycardia 3 (C). Each narrow QRS tachycardia was characterized by a negative P wave in leads II, III, and aVF. Intracardiac tracings show that the RVA–HRA interval of Tachycardia 1 (200 ms) was similar as that of Tachycardia 2 (208 ms), whereas that of Tachycardia 3 (108 ms) was significantly different. CS 1–2, distal coronary sinus electrogram; CS 15–16, proximal coronary sinus electrogram; His–d, distal His bundle electrogram; HRA–d, distal high right atrium electrogram; HRA–p, proximal high right atrium electrogram; RVA, right ventricular apex electrogram.

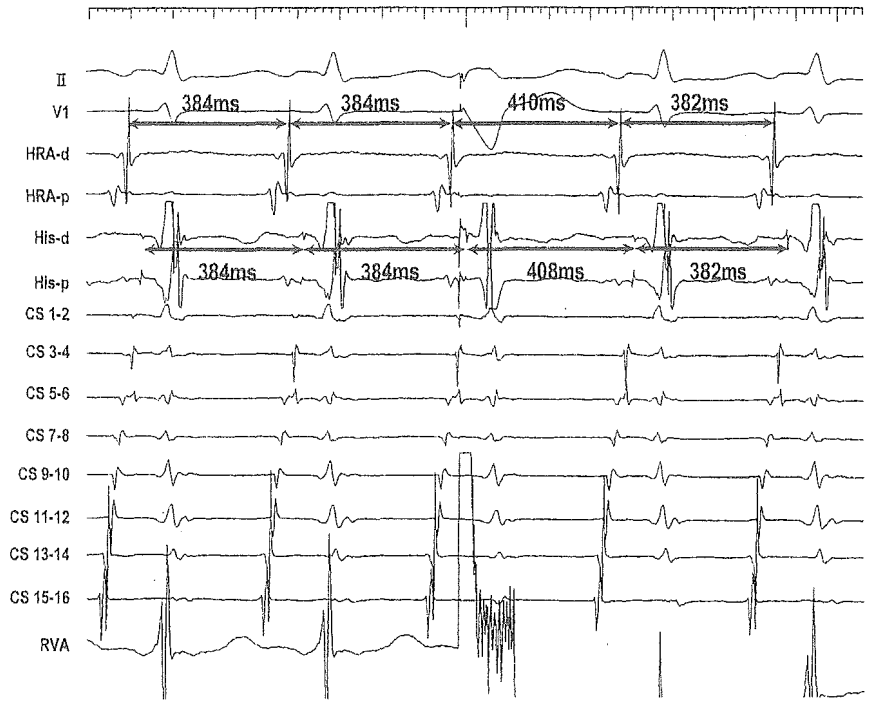


Fig 2. Simultaneous recording of ECG and intracardiac bipolar electrograms during Tachycardia 1 show the "postexcitation" phenomenon. A single ventricular extrastimulus, which was introduced from the RVA when the His bundle was refractory, delayed the subsequent atrial activation ("postexcitation" phenomenon). CS 1–2, distal coronary sinus electrogram; CS 15–16, proximal coronary sinus electrogram; His–d, distal His bundle electrogram; His–p, proximal His bundle electrogram; HRA–d, distal high right atrium electrogram; HRA–p, proximal high right atrium electrogram; RVA, right ventricular apex electrogram.

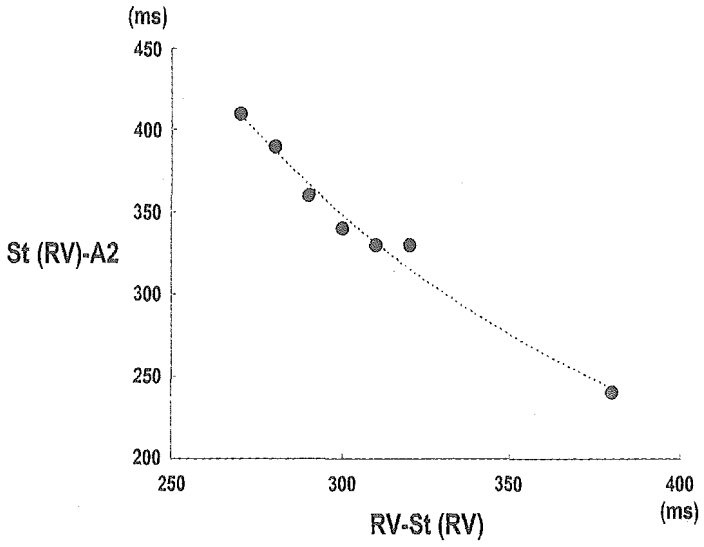


Fig 3. Retrograde VA conduction time curve obtained by a single ventricular extrastimulus during Tachycardia 1. Shortening of the coupling intervals of the extrastimulus (RV-St (RV)) resulted in increases in the retrograde VA conduction time (St (RV)-A2) during Tachycardia 1. A2, subsequent atrial activation; RV, right ventricular activation; St, stimulus.

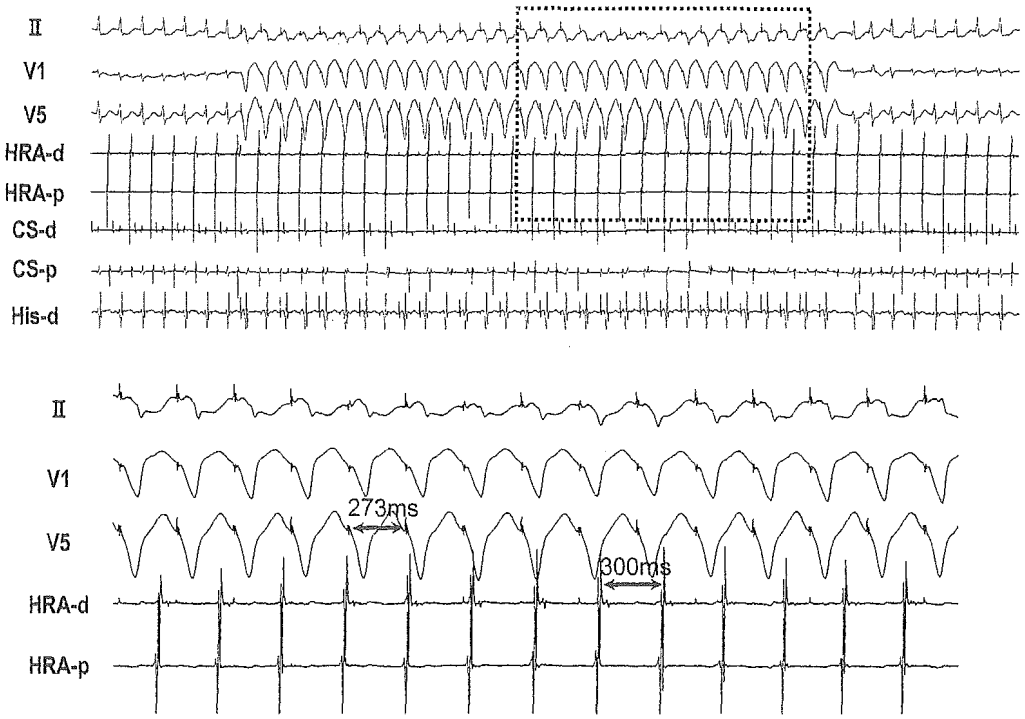


Fig 4. Simultaneous recording of ECG and intracardiac bipolar electrograms illustrate the AV dissociation by ventricular pacing during Tachycardia 3. Burst pacing (cycle length, 273 ms) from the RVA showed AV dissociation without affecting the cycle length of Tachycardia 3 (cycle length, 300 ms). CS–d, distal coronary sinus electrogram; CS–p, proximal coronary sinus electrogram; His–d, distal His bundle electrogram; HRA–d, distal high right atrium electrogram; HRA–p, proximal high right atrium electrogram; RVA, right ventricular apex.

no VA conduction after extrastimuli from the right ventricle, and none of the pacing protocols could induce the tachycardias, even with isoproterenol infusion. She has been clinically free from symptoms of palpitations during 2 years of follow-up.

## Discussion

PJRT is usually characterized by incessant forms of supraventricular tachycardia, and occasionally the development of tachycardia-induced cardiomyopathy[1–4] However, some reports have identified a paroxysmal type of PJRT, such as in the present patient[5,6] The electrocardiographic feature of PJRT is a narrow QRS tachycardia with a long RP' interval, but atypical forms of AVNRT and AT sometimes demonstrate similar electrocardiographic findings. In the present patient there were 3 types of narrow QRS tachycardia induced during the EPS. Tachycardia 1 was diagnosed as PJRT and Tachycardia 3 as AT, but Tachycardia 2 was not diagnosed precisely because of its spontaneous change to Tachycardia 3 or termination. However, the residual VA conduction by pacing from RVA showed a decremental property and the atrial activation sequence via the VA conduction was identical to that of Tachycardia 2.

Moreover, variable locations of the accessory pathway of PJRT, including the coronary sinus ostium and posterior mid-septum of the right atrium, have been reported.[7,8] Therefore, it is more likely that Tachycardia 2 was PJRT or an atypical form of AVNRT than AT.

We performed RFCA targeting the earliest atrial activation site during the tachycardias or via the VA conduction, which resulted in successful ablation of both arrhythmias.

*Acknowledgments*

*Dr Shimizu was supported in part by the Mitsubishi Pharma Research Foundation, Health Sciences Research Grants from the Ministry of Health, Labor, and Welfare, and Research Grants for Cardiovascular Diseases (15C-6) from the Ministry of Health, Labor and Welfare, Japan.*

## References

1. Gallagher JJ, Sealy WC. The permanent form of junctional reciprocating tachycardia: Further elucidation of the underlying mechanism. *Eur J Cardiol* 1978; **8:** 413–430.
2. Chien WW, Cohen TJ, Lee MA, Lesh MD, Griffin JC, Schiller NB, et al. Electrophysiological findings and long-term follow-up of patients with the permanent form of junctional reciprocating tachycardia treated by catheter ablation. *Circulation* 1992; **85:** 1329–1336.
3. Dorostkar PC, Silka MJ, Morady F, Dick M II. Clinical course of persistent junctional reciprocating tachycardia. *J Am Coll Cardiol* 1999; **33:** 366–375.
4. Aguinaga L, Primo J, Anguera I, Mont L, Valentino M, Brugada P, et al. Long-term follow-up in patients with the permanent form of junctional reciprocating tachycardia treated with radiofrequency ablation. *Pacing Clin Electrophysiol* 1998; **21:** 2073–2078.
5. Guarnieri T, Sealy WC, Kasell JH, German LD, Gallagher JJ. The non-pharmacologic management of the permanent form of junctional reciprocating tachycardia. *Circulation* 1984; **69:** 269–277.
6. Yagi T, Ito M, Odakura H, Namekawa A, Otomo J, Ishida A. Electrophysiologic comparison between incessant and paroxysmal tachycardia in patients with permanent form of junctional reciprocating tachycardia. *Am J Cardiol* 1996; **78:** 697–700.
7. Ticho BS, Saul JP, Hulse JE, De W, Lulu J, Walsh EP. Variable location of accessory pathways associated with the permanent form of junctional reciprocating tachycardia and confirmation with radiofrequency ablation. *Am J Cardiol* 1992; **70:** 1559–1564.
8. Shih HT, Miles WM, Klein LS, Hubbard JE, Zipes DP. Multiple accessory pathways in the permanent form of junctional reciprocating tachycardia. *Am J Cardiol* 1994; **73:** 361–367.

Drug Metab. Pharmacokinet. 20 (6): 423–427 (2005).

**Regular Article**

# *Stereoselective Effect of Amiodarone on the Pharmacokinetics of Racemic Carvedilol*

Kyoko FUKUMOTO[1], Takashi KOBAYASHI[1], Kazuo KOMAMURA[2], Shiro KAMAKURA[2], Masafumi KITAKAZE[2] and Kazuyuki UENO[1]*

[1]*Department of Pharmaceutical Sciences, Niigata University of Pharmacy and Applied Life Sciences, Niigata, Japan.* [2]*Departments of Research and* [3]*Cardiology, National Cardiovascular Center, Osaka, Japan*

Full text of this paper is available at http://www.jstage.jst.go.jp/browse/dmpk

**Summary:** We investigated whether there was a stereoselective effect of amiodarone on the pharmacokinetics of carvedilol. Among a series of 106 inpatients with heart failure, 52 received carvedilol monotherapy (carvedilol group) and 54 received carvedilol plus amiodarone (carvedilol + amiodarone group). The serum carvedilol concentration administered/dose ratio was compared between the two groups based on HPLC measurement of the serum levels of carvedilol, amiodarone, and desethylamiodarone. In 6 patients from the carvedilol group, serum carvedilol levels were compared before and after coadministration of amiodarone. There was no significant between-group difference of the serum concentration to dose (C/D ratio) for the R-enantiomer carvedilol, however, the C/D ratio for the S-enantiomer and the serum S-carvedilol to R-carvedilol (S/R) ratio were both significantly lower in the carvedilol group than in the carvedilol + amiodarone group($47.8 \pm 56.7$ versus $95.3 \pm 105$ ng/mg/kg, $P = 0.0048$ and $0.460 \pm 0.207$ versus $0.879 \pm 0.377$ ng/mg/kg, $P < 0.001$), respectively. Furthermore, the mean S-carvedilol concentration over 14 days of coadministration with amiodarone was higher than that before coadministration ($6.54 \pm 1.73$ ng/mL versus $3.03 \pm 0.670$ ng/mL, $P < 0.001$). These results suggest that metabolism of S-carvedilol was markedly inhibited by coadministration of amiodarone.

**Key words: carvedilol; amiodarone; stereoselective; interaction; pharmacokinetics**

## Introduction

Amiodarone is a class III antiarrhythmic agent (Vaughan William's classification),[1,2] which is widely used for the prevention of sustained ventricular tachycardia and ventricular fibrillation.[3-5] Until recently, however, concerns about potentially dangerous noncardiac side effects and its complex pharmacokinetics have limited the use of amiodarone to patients with the most drug-resistant and high-risk arrhythmias.[6] Nonetheless, amiodarone appears to significantly improve the prognosis after myocardial infarction,[7] and it has begun to be accepted as first-line therapy rather than being seen as a "last-chance" drug. This increase in popularity is evidenced by the rapidly growing use of amiodarone for management of refractory atrial arrhythmias. Amiodarone is predominantly metabolized to desethylamiodarone by cytochrome P 450(CYP)3A4 and CYP2C8, after which desethylamiodarone is further metabolized by CYP3A4.[8,9] Amiodarone has unique pharmacokinetic properties and interactions with various drugs,[10,11] including warfarin,[12-14] phenytoin,[15-17] flecainide,[18-20] and cyclosporine.[21,22] An *in vitro* study showed that amiodarone weakly inhibited CYP activity, while desethylamiodarone strongly inhibited the catalytic activity of CYP2C9, CYP2D6, and CYP3A4.[8]

The $\beta$-adrenegic receptor antagonists ($\beta$-blockers) are widely used to treat hypertention, angina, and heart failure. Among these drugs, the popularity of carvedilol has increased recently, because it is also useful for chronic heart failure. Carvedilol is a racemic mixture of R(+)- and S(−)-enantiomers that is mainly metabolized by CYP2D6; as well as also being partially metabolized by CYP1A2 and CYP2C9.[23,24] Carvedilol is often coadministered with amiodarone during treatment of arrhythmias or heart failure. Therefore, investigation of pharmacokinetic interactions between carvedilol and

*Received; July 2, 2005, Accepted; September 29, 2005*

**To whom correspondence should be addressed*: Kazuyuki UENO, Ph.D. Prof., *Department of Pharmaceutical Sciences, Niigata University of Pharmacy and Applied Life Sciences, 5-13-2, Kamishin'ei-cho, Niigata, 950-2081 Japan. Tel. & Fax. +81-25-268-1250, E-mail: uenok@niigata-pharm.ac.jp*

amiodarone is important in order to optimize the efficacy and safety of such therapy. The aim of this study was to investigate the stereoselectivity of the effect of amiodarone on the pharmacokinetics of carvedilol.

## Methods

**Subjects:** The subjects were a series of Japanese inpatients with heart failure who received treatment with amiodarone or carvedilol from January 2002 to December 2003 at the National Cardiovascular Center. All of the patients had stable symptoms of heart failure and were in New York Heart Association (NYHA) classes I to II. Fifty-two inpatients received maintenance carvedilol therapy (CAR group). Their mean age and body weight were 58.1 ± 16.9 years and 57.1 ± 10.0 kg (mean ± SD), respectively. Another 54 inpatients received combined maintenance therapy with carvedilol and amiodarone (CAR + AMD group). Their mean age and body weight were 52.6 ± 16.5 years and 58.2 ± 14.2 kg (mean ± SD), respectively. They received a fixed maintenance dose of amiodarone (twice a day, at 0700 and 1900) for at least 3 months. All patients also received a fixed maintenance dose of carvedilol (once a day, at 0700) for at least 2 weeks. Because all of the subjects were inpatients, compliance was ensured through administration of the drugs by a nurse, pharmacist, or cardiologist. To determine the serum concentrations of carvedilol enantiomers, amiodarone, and desethylamiodarone, blood samples were collected at 0700 hours from an arm vein. In 6 patients from the CAR group, amiodarone was added to the regimen and blood samples were obtained before and after 14 days of amiodarone therapy.

None of the patients had significant renal or hepatic disease or concomitant infection, and no adverse reactions or clinical complications were observed during this study. None of the subjects were receiving catecholamine preparations or any other drugs that might have influenced the pharmacokinetics of carvedilol (eg, rifampicin, phenobarbital, propafenone, or bucolome.[25]) Blood samples were centrifuged at 3000 × g for 10 minutes, and the serum thus obtained was stored at −30°C until analysis. Written informed consent was obtained from all patients before enrollment in this study.

**Materials:** Amiodarone was purchased from Wako Pure Chemical Industries, Ltd. (Osaka, Japan). Carvedilol (both enantiomers), desethylamiodarone and propfol were supplied by Roche Diagnostics Co. Ltd., Sanofi-Synthelabo Co. Ltd. and AstraZeneka Co. Ltd., respectively. Acetonitrile and methanol were of reagent grade for HPLC, while the other reagents were of reagent grade and were used without further purification.

**Assays:** Serum levels of the enantiomers of carvedilol were determined by high-performance liquid chromatography with propofol as the internal standard (IS). A serum sample (1 mL) was combined with the IS solution and 1 mL of 1 M NaOH. Then 5 mL of diethylether was added, and the resultant mixture was shaken for 10 min and centrifuged at 3000 × g for 5 min. After the upper layer was taken and evaporated in vacua; the residue was dissolved in methanol before injection into the HPLC system (LC-10ADVP, Shimadzu Corp. Kyoto, Japan). This system consisted of a reverse-phase column (Chiral OD-RH column, Daicel Chemical Industries Ltd, Osaka, Japan) and a fluorescence detector (excitation at 240 nm and emission at 340 nm). The mobile phase consisted of 0.044 M potassium phosphate buffer (pH 7.0) containing 0.5% triethylamine and acetonitrile (90:10 by volume), and the flow rate was set at 1.2 mL/min. The retention times of S-carvedilol, R-carvedilol and the IS were 16.5, 19.1, and 6.8 min, respectively. The lowest measurable concentration was 0.5 ng/mL. Inter-day and intra-day variations were less than 5%.

Serum amiodarone and desethylamiodarone concentrations were determined by HPLC with amitripylline as the IS.[26] In brief, amiodarone and desethylamiodarone were extracted with diethylether (pH 4), followed by evaporation, and the residue was dissolved in methanol before injection into the HPLC system. The system consisted of a reverse-phase column (Shimpack CLC-ODS, Shimadzu Corp, Kyoto, Japan) and an ultraviolet absorbance detector operating 242 nm. The mobile phase was a mixture of methanol, water, and 28% ammonia water (91:8.8:0.2 by volume), and the flow rate was set at 1.2 mL/min. The retention times of amiodarone, desethylamiodarone, and the IS were 21, 13, and 6 min, respectively. The lowest measurable concentration was 50 ng/mL. Inter-day and intra-day variations were less than 5%.

**Pharmacokinetic analysis:** All patients were administered a fixed maintenance dose of carvedilol for at least 2 weeks, so it was assumed that their serum carvedilol concentrations had reached steady-state. The sampling time for all subjects was set at 0700 h. Therefore, to evaluate pharmacokinetic parameters in the two groups, the ratio of the serum carvedilol concentration to the dose of carvedilol administered (C/D ratio) was used instead of oral clearance in this study. This ratio was calculated with C as the serum carvedilol concentration and D as the daily dose of racemic carvedilol (divided by 2 to obtain the dose of each enantiomer).

## Statistical Analysis

Data are presented as the mean ± standard deviation (SD). Statistical analysis was performed using one-way ANOVA and significance was set at $p < 0.05$.

## Results

The subjects received amiodarone and/or carvedilol for treatment of heart failure. No difference of NYHA class was observed between the two groups. **Tables 1 and 2** show a comparison of clinical characteristics and the pharmacokinetic parameters of carvedilol between the CAR group and the CAR + AMD group. There was a significant difference of the C/D ratio of S-carvedilol between the two groups; as well as the ratio of the S-carvedilol concentration to the R-carvedilol concentration (S/R ratio).

**Table 1.** Comparison of clinical characteristics and carvedilol dose between the CAR group and the CAR + AMD group.

| Parameter | CAR group | CAR + AMD group | P value |
|---|---|---|---|
| N | 52 | 54 | |
| Age (yr) | 58.1 ± 16.9 | 52.6 ± 16.5 | NS |
| BW (kg) | 57.1 ± 10.0 | 58.2 ± 14.2 | NS |
| Dose/BW (mg/kg) | 0.179 ± 0.118 | 0.144 ± 0.0926 | NS |

CAR, carvedilol; AMD, amiodarone; Dose, daily dose of carvedilol; BW, body weight; The CAR group received carvedilol monotherapy. The CAR + AMD group received combined carvedilol and amiodarone therapy. Data are shown as the mean ± standard deviation. NS, not significant.

**Table 2.** Comparison of the pharmacokinetic parameters of carvedilol enantiomers between the CAR group and the CAR + AMD group.

| Parameter | CAR group | CAR + AMD group | P value |
|---|---|---|---|
| N | 52 | 54 | |
| Total C/D | 196 ± 282 | 210 ± 232 | NS |
| S-C/D | 47.8 ± 56.7 | 95.3 ± 105 | < 0.01 |
| R-C/D | 149 ± 226 | 123 ± 137 | NS |
| S/R ratio | 0.460 ± 0.207 | 0.879 ± 0.377 | < 0.001 |

CAR, carvedilol; AMD, amiodarone; C/D, the serum carvedilol concentration/dose ratio; S,S-carvedilol; R,R-carvedilol; S/R ratio, ratio of the S-carvedilol concentration to the R-carvedilol concentration. The CAR group received carvedilol monotherapy. The CAR + AMD group received combined carvedilol and amiodarone therapy. Data are shown as the mean ± standard deviation. NS, not significant.

**Table 3** shows a comparison of carvedilol enantiomer concentrations before and after 14 days of coadministration with amiodarone. The mean S-carvedilol concentration and the S/R ratio were higher after coadministration compared with before coadministration (S-carvedilol, before 3.03 ± 0.670 ng/mL; after 6.54 ± 1.73 ng/mL; $P < 0.001$; S/R ratio, before 0.380 ± 0.117; after 0.734 ± 0.153; $P < 0.001$).

## Discussion

In this study, the subjects received amiodarone and/or carvedilol therapy for the treatment of heart failure. It is well known that the severity of heart failure influences drug dispositions[27], but no difference of NYHA class was observed between the two groups. Therefore, it seemed reasonable to suggest that the influence of heart failure could be ignored.

Carvedilol is a racemic mixture of S- and R-enantiomers. Metabolism of S-carvedilol is generally more rapid than that of R-carvedilol both *in vitro* and *in vivo*. S-carvedilol is predominantly metabolized through hydroxylation by CYP2D6, CYP2C9, and CYP1A2, as well as demethylation by CYP2C9.[23,24] On the other hand, R-carvedilol is predominantly metabolized through hydroxylation by CYP2D6 and CYP1A2. As shown in **Table 2**, there were no significant difference in the C/D ratio of R-carvedilol between the CAR group and the CAR + AMD group, but the C/D ratio of S-carvedilol was significantly higher in the CAR + AMD group than in the CAR group and the S/R ratio was significantly greater in the CAR + AMD group than in the CAR group. As shown in **Table 3**, although the mean R-carvedilol concentration was not altered by coadministration with amiodarone, the mean S-carvedilol concentration and the S/R ratio were significantly increased by coadministration. These results suggested that metabolism of S-carvedilol was markedly

**Table 3.** Carvedilol enantiomer concentrations before and after 14 days of coadministration with amiodarone in 6 subjects.

| Parameter | Before | After | P value |
|---|---|---|---|
| Carvedilol | | | |
| Dose (mg/day) | 12.1 ± 5.1 | 12.1 ± 5.1 | — |
| Total concentration (ng/mL) | 11.9 ± 4.28 | 15.9 ± 4.72 | NS |
| S-carvedilol concentration (ng/mL) | 3.03 ± 0.670 | 6.54 ± 1.73 | < 0.001 |
| R-carvedilol concentration (ng/mL) | 8.82 ± 3.76 | 9.31 ± 3.23 | NS |
| S/R ratio | 0.380 ± 0.117 | 0.734 ± 0.153 | < 0.001 |
| Amiodarone | | | |
| Dose (mg/day) | | 117 ± 40.8 | |
| Amiodarone concentration (μg/mL) | | 0.314 ± 0.119 | |
| Desethylamiodarone concentration (μg/mL) | | 0.238 ± 0.0857 | |

Age, 52.7 ± 14.7 yr; Body Weight, 55.3 ± 12.5 kg, S/R ratio, ratio of the S-carvedilol concentration to the R-carvedilol concentration. Data are the mean ± standard deviation. NS, not significant.

inhibited by coadministration of amiodarone.

Amiodarone is known to show pharmacokinetic interactions with various drugs. An *in vitro* study showed that amiodarone weakly inhibits CYP activity, with an inhibition constant (Ki) ranging from 45.1 to 27.6 $\mu$M, while desethylamiodarone competitively inhibits the catalytic activity of CYP2D6 (Ki = 4.5 $\mu$M) and noncompetitively inhibits CYP3A4. The catalytic activity of CYP2C9 (Ki = 2.3 $\mu$M) shows mixed inhibition by desethylamiodarone.[8] Thus, desethyamiodarone had a markedly greater inhibitory effect on CYP2C9 than on CYP2D6 or CYP3A4. The S-enantiomer of carvedilol is a major substrate of CYP2C9, but the R-enantiomer is not. These findings suggest that the difference between the effect of amiodarone on metabolism of S-carvedilol and R-carvedilol was related to a difference in the affinity of the two enantiomers for CYP2C9 and a difference in the inhibitory mechanisms acting on CYP2C9 and CYP2D6. On the other hand, it has been reported that intestinal expression of P-glycoprotein (P-gp) and multidrug resistance protein (MRP2) are the major influences on the disposition of carvedilol.[28] Amiodarone is also a substrate of P-gp, and desethylamiodarone was a strong in vitro inhibitor of P-gp than amiodarone itself.[29] Therefore, the differential effects of amiodarone on the disposition of S-carvedilol and R-carvedilol may be related to a difference in the affinity of the two enantiomers for P-gp. However, no reports have been published about a difference in the P-gp affinity of these two enantiomers.

Carvedilol is a mixed $\alpha$- and $\beta$-adrenergic receptor antagonist. Although each enantiomer shows equally potent $\alpha$-blockade, the S-enantiomer is principally responsible for $\beta$-blockade.[30] In this study, the effect of amiodarone on the clearance of R-carvedilol was negligible, but its influence on that of S-carvedilol was considerable. Also, although no significant between -group difference was observed in the mean dose relative to body weight (dose/BW) ratio; it tend to be lower in the CAR + AMD group than in the CAR group ($P = 0.091$). Therefore, when amiodarone is administered to patients on maintenance carvedilol therapy, it is necessary to monitor a potential increase of $\beta$-blockade caused by a rise of the serum S-carvedilol concentration. Therefore, when carvedilol and amiodarone are administered together, not only the pharmacokinetics of carvedilol but also its pharmacodymanics may be altered.

In conclusion, when carvedilol and amiodarone are coadministered, it is necessary to be aware that S-carvedilol clearance may be markedly decreased due to inhibition of CYP2C9 by desethylamiodarone. More detailed studies on the mechanism of this interaction are needed in the future.

## References


1) Vaughan Williams, E. M.: Significance of classifying antiarrhythmic actions since the cardiac arrhythmia suppression trial. *J. Clin. Pharmacol.*, **31**: 123–135 (1991).
2) Vaughan Williams, E. M.: A classification of antiarrhythmic actions reassessed after a decade of new drugs. *J. Clin. Pharmacol.*, **24**: 129–147 (1984).
3) Gill, J., Heel, R. C. and Fitton, A.: Amiodarone. An overview of its pharmacological properties, and review of its therapeutic use in cardiac arrhythmias. *Drugs*, 43: 69–110 (1992).
4) Lesko, L. J.: Pharmacokinetic drug interactions with amiodarone. *Clin. Pharmacokinet.*, **17**: 130–140 (1989).
5) Latini, R., Tognoni, G. and Kates, R. E.: Clinical pharmacokinetics of amiodarone. *Clin. Pharmacokinet.*, **9**: 136–156 (1984).
6) Singh, B. N.: Amiodarone: the expanding antiarrhythmic role and how to follow a patient on chronic therapy. *Clin. Cardiol.*, **20**: 608–618 (1997).
7) Estes, N. A. 3rd., Weinstock, J., Wang, P. J., Homoud, M. K. and Link, M. S.: Use of antiarrhythmics and implantable cardioverter-defibrillators in congestive heart failure. *Am. J. Cardiol.*, **91**: 45D-52D (2003).
8) Ohyama, K., Nakajima, M., Suzuki, M., Shimada, N., Yamazaki, H. and Yokoi T.: Inhibitory effects of amiodarone and its N-deethylated metabolite on human cytochrome P450 activities: prediction of *in vivo* drug interactions. *Br. J. Clin. Pharmacol.*, **49**: 244–253 (2000).
9) Ohyama, K., Nakajima, M., Nakamura, S., Shimada, N., Yamazaki, H. and Yokoi T.: A significant role of human cytochrome P450 2C8 in amiodarone N-deethylation: an approach to predict the contribution with relative activity factor. *Drug Metab. Dispos.*, **28**: 1303–1310 (2000).
10) Lesko, L. J.: Pharmacokinetic drug interactions with amiodarone. *Clin. Pharmacokinet.*, **17**: 130–140 (1989).
11) Marcus, F. I.: Drug interactions with amiodarone. *Am. Heart J.*, **106**: 924–930 (1983).
12) Heimark, L. D., Wienkers, L., Kunze, K., Gibaldi, M., Eddy, A. C., Trager, W. F. and *et al.*: The mechanism of the interaction between amiodarone and warfarin in humans. *Clin. Pharmacol. Ther.*, **51**: 398–407 (1992).
13) Watt, A. H., Stephens, M. R., Buss, D. C. and Routledge, P. A.: Amiodarone reduces plasma warfarin clearance in man. *Br. J. Clin. Pharmacol.*, **20**: 707–709 (1985).
14) Almog, S., Shafran, N., Halkin, H., Weiss, P., Farfel, Z., Martinowitz, U. and *et al.*: Mechanism of warfarin potentiation by amiodarone: dose-and concentration-dependent inhibition of warfarin elimination. *Eur. J. Clin. Pharmacol.*, **28**: 257–261 (1985).
15) Nolan, P. E. Jr., Marcus, F. I., Karol, M. D., Hoyer, G. L. and Gear, K.: Effect of phenytoin on the clinical pharmacokinetics of amiodarone. *J. Clin. Pharmacol.*, **30**: 1112–1119 (1990).
16) Nolan, P. E. Jr., Erstad, B. L., Hoyer, G. L., Bliss, M., Gear, K. and Marcus, F. I.: Steady-state interaction

between amiodarone and phenytoin in normal subjects. *Am. J. Cardiol.*, **65**: 1252–1257 (1990).
17) Nolan, P. E. Jr., Marcus, F. I., Hoyer, G. L., Bliss, M. and Gear, K.: Pharmacokinetic interaction between intravenous phenytoin and amiodarone in healthy volunteers. *Clin. Pharmacol. Ther.*, **46**: 43–50 (1989).
18) Shea, P., Lal, R., Kim, S. S., Schechtman, K. and Ruffy, R.: Flecainide and amiodarone interaction. *J. Am. Coll. Cardiol.*, 7: 1127–1130 (1986).
19) Haefeli, W. E., Bargetzi, M. J., Follath, F. and Meyer, U. A.: Potent inhibition of cytochrome P450IID6 (debrisoquine 4-hydroxylase) by flecainide in vitro and *in vivo*. *J. Cardiovasc. Pharmacol.*, **15**: 776–779 (1990).
20) Funck-Brentano, C., Becquemont, L., Kroemer, H. K., Buhl, K., Knebel, N. G., Eichelbaum, M. and *et al.*: Variable disposition kinetics and electrocardiographic effects of flecainide during repeated dosing in humans: contribution of genetic factors, dose-dependent clearance, and interaction with amiodarone. *Clin. Pharmacol. Ther.*, **55**: 256–269 (1994).
21) Nicolau, D. P., Uber, W. E., Crumbley, A. J. 3rd. and Strange, C.: Amiodarone-cyclosporine interaction in a heart transplant patient. *J. Heart Lung Transplant.*, **11**: 564–568 (1992).
22) Chitwood, K. K., Abdul-Haqq, A. J. and Heim-Duthoy, K. L.: Cyclosporine-amiodarone interaction. *Ann. Pharmacother.*, **27**: 569–571 (1993).
23) Oldham, H. G. and Clarke, S. E.: *In vitro* identification of the human cytochrome P450 enzymes involved in the metabolism of R(+)- and S(−)-carvedilol. *Drug Metabo. Dispos.*, **25**: 970–977 (1997).
24) Zhou, H. H. and Wood, A. J. J.: Stereoselective disposition of carvedilol is determined by CYP2D6. *Clin. Pharamcol. Ther.*, **57**: 518–524 (1995).
25) Matsumoto, K., Ishida, S., Ueno, K., Hashimoto, H., Takada, M., Kamakura, S. and *et al.* The stereoselective effects of bucolome on the pharmacokinetics and pharmacodynamics of racemic warfarin. *J. Clin. Pharmacol.*, **41**, 459–464 (2001).
26) Masaki, K., Ueno, K., Tsuji, M., Hiraki, K., Takada, M., Kamakura, S. and Shibakawa, M.: A simple assay for amiodarone and desethylamiodarone and its clinical application. *Jpn. J. Hosp. Pharm.*, **25**: 28–33 (1999).
27) Tenero, D., Boike, S., Boyle, D., Ilson, B., Fesniak, H. F., Brozena, S. and Jorkasky, D.: Steady-state pharmacokinetics of carvedilol and its enantiomers in patients with congestive heart failure. *J. Clin. Pharmacol.*, **40**: 844–853 (2000).
28) Giessmann, T., Modess, C., Hecker, U., Zschiesche, M., Dazert, P., Kunert-Keil, C., Warzok, R. and *et al.*: CYP2D6 genotype and induction of intestinal drug transpoters by rifampin predict presystemic clearance of carvedilol in healthy subjects. *Clinical. Pharmacol. Ther.*, **75**: 213–222 (2004).
29) Katoh, M., Nakajima, M., Yamazaki, H. and Yokoi, T.: Inhibitory effects of CYP3A4 substrates and their metabolites on P-glycoprotein-mediated transport. *Eur. J. Pharm. Sci.*, **12**: 505–513 (2001).
30) Bartsch, W., Sponer, G., Strein, K., Muller-Beckmann, B., Kling, L., Bohm, E. and *et al.*: Pharmacological characteristics of the stereoisomers of carvedilol. *Eur. J. Clin. Pharmacol.*, **38 Suppl 2**: S104–107 (1990).

Journal of Interventional Cardiac Electrophysiology 14, 183–192, 2005


# Assessment of Ability of Activation Mapping by Duodecapolar Catheter to Diagnose Complete Isthmus Block Utilizing Electroanatomical Mapping System

*Kiyoshi Otomo, Takashi Noda, Eiichiro Nakagawa, Kazuhiro Satomi, Wataru Shimizu, Kazuhiro Suyama, Takashi Kurita, Naohiko Aihara, and Shiro Kamakura*

*Division of Cardiology, National Cardiovascular Center, 5-7-1 Fujishirodai, Suita City, Osaka Prefecture, 565-8565, Japan*

*Abstract.* **Duodecapolar catheters (DPCs) have been widely used to diagnose isthmus block after ablation in patients with atrial flutters. The purpose of this study was to assess the ability of DPC to diagnose isthmus block utilizing electroanatomical mapping system (CARTO).**

***Methods*: Sixty-two patients with common atrial flutter underwent isthmus ablation during CS pacing while DPC was positioned at lateral wall of RA along tricuspid annulus (TA). When activation sequence of DPC recording changed exclusively counter-clockwise after ablation, or did not even after ablations targeting single potentials on ablation line (Ab-L), only lateral side of Ab-L was remapped using CARTO to assess whether complete block (CB) was established.**

***Results*: After ablation, DPC recording suggested CB and incomplete block (ICB) in 53 (85%) and 9 patients (15%), respectively. In 51/53 patients (96%) with CB suggested by DPC recordings, CARTO remap also demonstrated CB, however, in the remaining two patients (4%), demonstrated ICB with residual isthmus conduction that was slow enough to allow wavefront conducting around TA to arrive at distal dipole of DPC earlier, mimicking CB. In 4/9 patients (44%) with ICB suggested by DPC recordings, CARTO remap also demonstrated ICB, however, in the remaining five patients (56%), demonstrated CB with earlier arrival of wavefront traversing posterior wall at just lateral to Ab-L than that conducting around TA, mimicking ICB. Sensitivity, specificity, positive, and negative predictive values of DPC to diagnose CB were 91, 67, 96, and 44%, respectively.**

***Conclusions*: Mapping using DPC would not be sufficient for diagnosis of CB and ICB.**

*Key Words.* **atrial flutter, isthmus block, catheter ablation, electroanatomical mapping system, activation mapping**

## Introduction

The common type atrial flutter (AFL) has been treated with high successful rates by creating a complete line of bidirectional conduction block at the anatomical isthmus between the tricuspid annulus (TA) and the inferior vena cava (IVC) utilizing the radiofrequency (RF) energy [1,2]. During the ablation procedure, duodecapolar catheters (DPCs) have been widely used to confirm the clockwise conduction block at the isthmus by recognizing an exclusively descending activation sequence at the contralateral side of the right atrium (RA) during pacing from proximal coronary sinus (PCS) or low lateral RA (LLRA) (here called "the activation mapping") [1,2]. However, several studies have pointed out the diagnostic limitations of the activation mapping [3–7]. First, markedly slow isthmus conduction may not be detected by the activation mapping and may mimic the complete isthmus block [3,4]. Secondly, the transversal conduction across the crista terminalis (CT) may mimic the incomplete clockwise (CW) isthmus block due to pre-excitation of the lateral wall by the transversal wavefront across the CT despite the completion of the complete block [5–7]. The purpose of this study was to assess the ability of the activation mapping using the DPC positioned at lateral wall of the RA along the TA to diagnose the complete or incomplete isthmus block during PCS pacing utilizing the three-dimensional electroanatomical mapping system (CARTO) [8].

## Methods

### Patients

Sixty-two consecutive patients referred for the RF catheter ablation of drug-refractory common type AFL were studied prospectively. There were 55

Address for correspondence: Kiyoshi Otomo, MD, Department of Cardiovascular Medicine, Tokyo Medical and Dental University, 1-5-45 Yushima Bunkyo-ku, Tokyo, 113-8510, Japan. E-mail: kotomo.cvm@tmd.ac.jp

*Received 22 October 2004; accepted 13 September 2005*

males and 7 females, with the mean age of 66 ± 11 years. All patients had at least one ECG documentation of common type AFL prior to the ablation procedure, defined by negative sawtooth waves in II, III, and aVF with isoelectric positive patterns in V1. The mean number of priorly-failed antiarrhythmic drugs was 2.3 ± 1.2 per a patient. Twenty-two patients (35%) also had paroxysmal atrial fibrillation. Twenty-two patients (35%) had structural heart diseases including coronary heart disease ($n = 11$), valvular heart disease ($n = 6$), dilated cardiomyopathy ($n = 3$), and hypertrophic cardiomyopathy ($n = 2$).

### *Electrophysiological Study*

All patients gave written informed consents prior to the procedures. The antiarrhythmic agents had been discontinued for at least five half-lives before the procedures. Under local anesthesia, venous access was obtained from both femoral and antecubital veins to introduce three electrode catheters into the RA. Either a 6-French octapolar (2-2-2 mm interelectrode spacings, EP Technology) or a 2-French 16-polar catheter (Pathfinder, 2-5-2 mm inter-electrode spacings, Cardima) was inserted into the coronary sinus (CS) with its proximal dipole positioned at the ostium of CS. A 7-French DPC (Halo, 2-5-2 mm interelectrode spacing, Cordis-Webstar or Livewire, 2-5-2 mm interelectrode spacing, Daig) was positioned along the TA with its distal dipole positioned at just lateral region to or across the anticipated ablation line. Each catheter manipulator tried to position the DPC as close to the TA as possible in order to map the activation sequence of the lateral wall near the TA (Fig. 1). A 7-French 4 mm-tipped quadripolar ablation catheter with a magnetic field sensor located at the tip (NAVI-STAR, 2-2-2 mm interelectrode spacings, Biosence-Webster) was inserted into the RA and used for CARTO mapping and ablation. Bipolar electrograms were filtered through a bandpass of 30–500 Hz, displayed on a real-time monitor at a paper speed of 100 mm/s and stored with 2-kHz sampling frequency on magneto-optical disks (CardioLab system, Prucka Engineering Inc or Bard EP lab system). Before the RA mapping using the CARTO, the isthmus-dependency was confirmed by entrainment pacing, thereafter overdrive atrial pacing and/or external cardioversion were performed to restore sinus rhythm in patients with sustained AFL at the beginning of the electrophysiological study. In patients with sinus rhythm, AFL induction was not attempted.

### *CARTO Mapping Before Isthmus Ablation*

The whole RA was mapped using the CARTO during PCS pacing at the rate of 100–120 ppm. The time reference ($t = 0$) for activation time of each mapped site was set at the pacing stimulus delivered from the proximal dipole of the CS catheter located at the ostium of the CS. The CARTO map was displayed by constructing a three-dimensional shell of the RA with the isochronal expression of each local activation time by rainbow colors, that is, red, orange, yellow, green, blue, and purple, from early to late activation. The anatomic landmarks such as the TA, IVC, CT, superior vena cava, and His bundle were labeled on the RA map by using

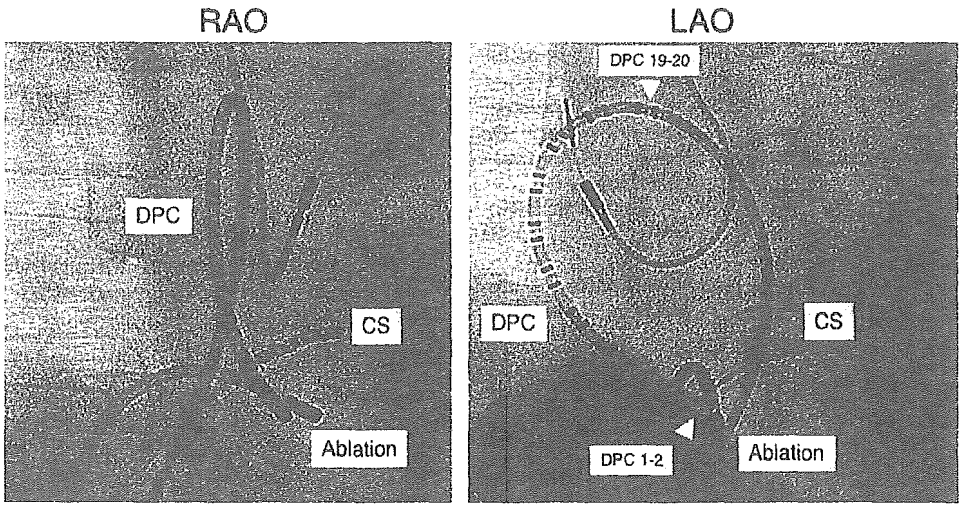


*Fig. 1. Catheter Position during the study in right (RAO) and left anterior oblique (LAO) fluoroscopic projections. DPC = duodecapolar catheter; CS = coronary sinus.*

different color tags. The fill threshold was preset at 10 mm.

### *RF Catheter Ablation of TA-IVC Isthmus*

The catheter ablation was performed linearly at the TA-IVC isthmus by sequential point-by-point deliveries of the RF energy during PCS pacing. The ablation was started from the TA edge with large ventricular and small atrial electrograms, and completed at the IVC edge. The ablation line was set at around 6 o'clock position of the TA. Using the Medtronic Atakr RF pulse generator, the 550 kHz unmodulated current was delivered between the distal tip of the ablation catheter and the indifferent patch electrode positioned at the back of the patient in a temperature-controlled mode with the upper temperature limit of 60°C, the maximal power output of 40 Watt and the duration of 60 s or less for each application. Each ablation site was labeled on the CARTO map as a dark red tag.

If the activation sequence of the lateral wall recorded by the DPC had changed exclusively CCW after one linear isthmus ablation, remapping was performed by the CARTO. If the activation sequence of the lateral wall had not changed exclusively CCW after one linear isthmus ablation, further RF energy applications were performed targeting single or fragmented potentials on the previous ablation line until an exclusively CCW activation sequence was observed in the DPC recording. If an exclusively CCW activation sequence was not obtained even after multiple ablations targeting single or fragmented potentials on the previous ablation line, the remapped was performed using the CARTO.

### *Remapping After Isthmus Ablation by CARTO*

After the isthmus ablation, the ablation line and the region lateral to it were remapped using CARTO to examine whether the complete isthmus block had been achieved [8]. The remapping was started by obtaining several points on the ablation line and at just lateral region along the ablation line, and then progressively more lateral region was remapped. At sites with double potentials on the ablation line, the second component was considered to reflect the local activation of just lateral region to the ablation line, so local activation was measured at the timing of the second component. The sites with triple or fragmented potentials on the ablation line were not included in the CARTO remap, because the local activation time of these sites were unclear. The fill threshold was preset at 10 mm.

## *Definitions*

### *Activation Sequence of DPC*

After the isthmus ablation, the activation sequence of the atrial electrograms recorded from the DPC was evaluated and classified into two patterns. "The exclusively CCW pattern," which conventionally suggests the complete CW isthmus block, was defined as the fully-descending activation pattern with the latest activation at the dipole just lateral to the ablation line. "The collision pattern," which conventionally suggests the incomplete CW isthmus block, was defined as the collision of the ascending and descending wavefronts at the lateral wall.

### *Remapping by CARTO*

The CARTO remaps were evaluated in terms of the presence or absence of early breakthroughs from the ablation line propagating in the septal-to-lateral direction during PCS pacing. "The complete CW block" was defined as a situation where there was no early breakthrough from the ablation line. "The incomplete CW block" was defined as a situation where there was an early breakthrough from the ablation line propagating in the septal-to-lateral direction.

### *Statistical Analysis*

The continuous variables were expressed as mean ± SD, and the comparisons were made using Mann–Whitney $U$ test. A $p$ value of less than 0.05 was considered statistically significant.

## *Results*

Among all 62 patients, 25 patients (40%) were in AFL and the others 37 patients (60%) were in sinus rhythm at the beginning of the procedure. In all patients with AFL, the isthmus was confirmed to be involved in the reentrant circuit of AFL by entrainment pacing, thereafter sinus rhythm was restored by overdrive atrial pacing or external electrical cardioversion before the CARTO mapping.

### *CARTO Mapping Before Isthmus Ablation*

In each patient, the RA map was constructed utilizing the CARTO during PCS pacing (pacing cycle length 520 ± 40 ms) with a mean of 126 ± 46 points per a map and showed the intact CW isthmus conduction and the collision of the CW and CCW wavefronts at the lateral wall before the ablation. The activation sequence in the DPC recordings showed the collision pattern in all patients.

*Table 1. The results of the DPC recordings and the CARTO remaps after isthmus ablation*

| | Activation sequence of DPC recording | | |
|---|---|---|---|
| | Exclusively CCW pattern | Collision pattern | Total |
| CARTO remap | | | |
| Complex CW block | 51 | 5 | 56 |
| Incomplete CW block | 2 | 4 | 6 |
| Total | 53 | 9 | 62 |

CW: clockwise; CCW: counter-clockwise; DPC: duodecapolar catheter.

### *Isthmus Ablation and Activation Mapping Using DPC*

Fifty-three patients (85%) showed the exclusively CCW pattern after 143 applications of the RF energy, while the remaining nine patients (15%) showed the collision pattern even after 2514 applications of the RF energy (Table 1). In four patients with the collision pattern, single or fragmented potentials remained to be recorded on the ablation line even after 385 times of RF energy applications and finally could not be abolished. In the remaining five patients with the collision pattern, although single or fragmented potentials were abolished from the ablation line after 132 times of RF energy applications, shortly-split double potentials remained to be recorded all along the ablation line. The mean interval from the pacing stimulus to the atrial electrogram recorded just lateral to the ablation line was 16 ± 242 among those with the exclusively CCW pattern and was 97 ± 27 ms among those with the collision pattern, respectively ($P < 0.05$).

### *CARTO Remapping After Isthmus Ablation*

Remapping after the isthmus ablation showed the complete CW block in 56 patients (90%), whereas the incomplete CW block in the remaining six patients (10%) (Table 1). Among those with the incomplete CW block, the conduction gaps on the ablation lines were localized to tricuspid annular ($n = 1$), middle ($n = 2$) and inferior vena caval one thirds of the isthmi ($n = 3$).

## *Comparisons of Results from Activation Mapping Using DPC and CARTO Remapping*

### *Patients with Exclusively CCW Pattern in DPC*

Of 53 patients with the exclusively CCW pattern in the DPC recordings, 51 patients (96%) showed the complete CW block, whereas the other two patients (4%) showed the incomplete CW block in the CARTO remaps (Table 1 and Fig. 2). In all 51 patients with the complete CW isthmus block, a corridor of widely-split double potentials with the mean inter-potential interval of 120 ± 23 ms was recorded all along the ablation line. In two patients with the incomplete CW isthmus block, the CARTO remap showed the markedly slow trans-isthmus conduction with an early breakthrough from the IVC edge of the ablation line, where fractionated potentials of long durations (95 and 110 ms) were recorded (Fig. 3, left). From the other part of the ablation line, shortly-split double potentials were recorded (mean inter-potential interval: 75 ms). At the tricuspid annular side of the isthmus where the DPC was positioned, however, a wavefront propagating counter-clockwisely along the TA arrived at the just lateral region to the ablation line before the collision with the trans-isthmus wavefront (Fig. 2, right and Fig. 3, right). These inconsistent results between the activation mapping using the DPC and the remapping using the CARTO turned out due to the longitudinally dissociated activation pattern within the isthmus, that is, the CCW activation pattern in the tricuspid annular side and the CW activation pattern in the IVC side of the isthmus. In both patients, an additional RF application at the conduction gap resulted in the appearance of a widely-split double potential at the ablation site without a change in the activation sequence of the DPC recording, and the complete CW block was demonstrated by the CARTO remapping (not shown). In all patients with exclusively CCW pattern, complete CCW block was also confirmed by remapping the septal region during LLRA pacing using CARTO (not shown).

### *Patients with Collision Pattern in DPC*

Among nine patients with the collision pattern in the DPC recordings, four patients (44%) showed the incomplete CW block, whereas the other five patients (56%) showed the complete CW block (Table 1 and Fig. 4). Among all five patients with the complete CW block, the CARTO remap showed an early wavefront from the posterior wall of the RA, arriving at the ablation line earlier than a CCW wavefront along the TA and propagating in the septal-to-lateral direction along the isthmus to collide with the CCW periannular wavefront at the lateral wall (Fig. 4, right). In these five

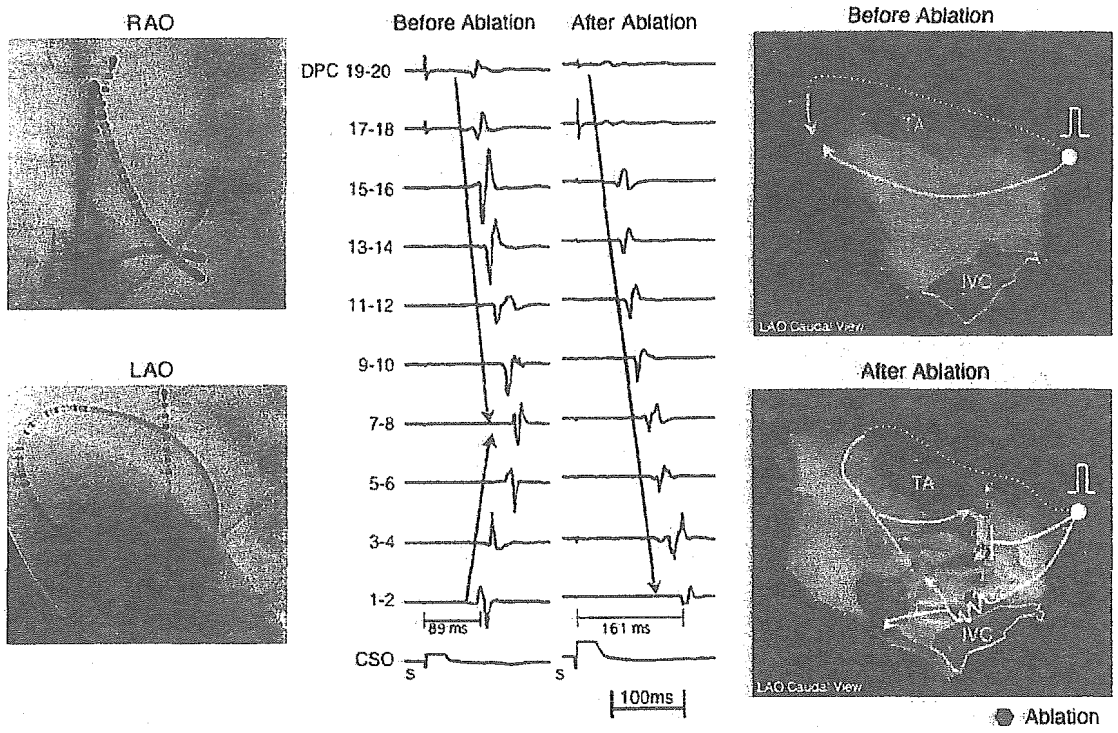


***Fig. 2.*** *The catheter position (left panel), the intracardiac recordings from the DPC and the CS catheter during PCS pacing with the cycle length of 500 ms before and after the isthmus ablation (middle panel) and the CARTO maps of the RA during PCS pacing before and after ablation (right panel) in a patient with an exclusively CCW activation pattern in the DPC recording in spite of incomplete isthmus block.* ***Left panel,*** *The distal dipole of the DPC was positioned near the TA just lateral to the ablation line.* ***Middle panel,*** *The activation pattern of the DPC changed from the collision pattern (left, before ablation) to the exclusively CCW pattern (right, after ablation). The interval from the pacing stimulus to the atrial electrogram at DPC 1-2 prolonged after the ablation.* ***Right panel,*** *Before the isthmus ablation, the CW and CCW wavefronts collided at the lateral wall (upper). The remapping after one linear isthmus ablation showed the incomplete isthmus block with the longitudinally dissociated intra-isthmus conduction due to the markedly slow trans-isthmus conduction (shown by red region). CSO: ostium of coronary sinus; DPC: duodecapolar catheter; IVC: inferior vena cava; S: pacing stimulus; TA: tricuspid annulus.*

patients, further mapping along the IVC orifice revealed these inconsistent results between the DPC recordings and the CARTO remaps were due to the earlier wavefronts conducting transversally across the CT (Fig. 5). Among them, shortly-split double potentials with the mean interpotential interval of 5,012 ms were recorded all along the ablation lines (Fig. 6, left). The remapping of septal region during LLRA pacing also confirmed complete CCW isthmus block in all five patients with complete CW block and incomplete CCW isthmus block in all four patients with incomplete CW block (not shown).

## *Ability of Activation Mapping Using DPC to Diagnose Isthmus Block*

The ability of the activation mapping using the DPC to diagnose the CW isthmus block was summarized in Table 2. The sensitivity, specificity, positive, and negative predictive values of the exclusively CCW pattern in the DPC recording during PCS pacing after the isthmus ablation to diagnose the complete CW block were 91.1, 66.7, 96.2, and 44.4%, respectively.

## *Discussion*

As far as we have acknowledged, this is the first study that both prospectively and globally assessed the ability of the activation mapping using DPCs to diagnose the isthmus block utilizing

***Table 2.*** *The diagnostic ability of activation mapping utilizing the DPC*

| | |
|---|---|
| Sensitivity | 91.1% |
| Specificity | 66.7% |
| Positive predictive value | 96.2% |
| Negative predictive value | 44.4% |

DPC: duodecapolar catheter.

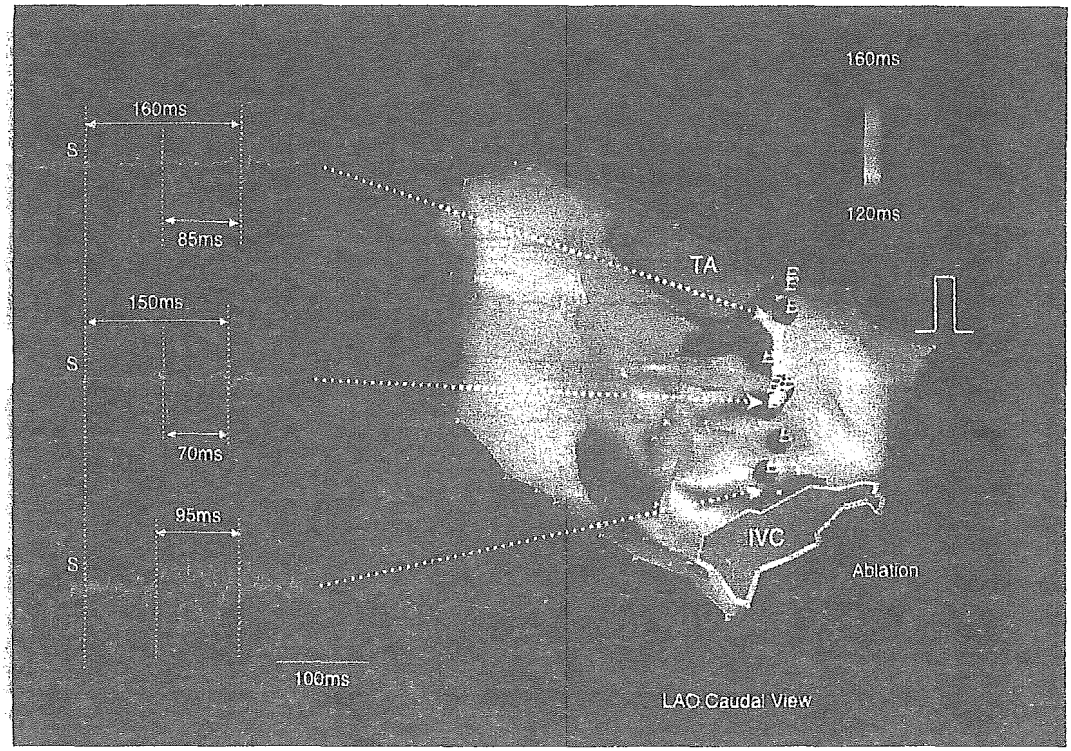


*Fig. 3. A CARTO remap after the isthmus ablation during PCS pacing viewed from left anterior oblique (LAO) caudal projection (right), and the bipolar electrograms recorded on the ablation line (left) in the same patient as in Fig. 2.* ***Right panel****, The residual isthmus conduction was depicted as a red region at the IVC edge of the ablation line. The direction of the wavefront activation was dissociated within the isthmus between the tricuspid annular and the inferior vena caval parts. The color bar indicates the activation time of each site, depicting the earliest activation site as red and the latest activation site as purple.* ***Left panel****, Shortly-split double potentials were recorded on the ablation line at the tricuspid annular side and the middle region, respectively. From the conduction gap at the inferior vena caval part of the ablation line, a fragmented potential with long duration was recorded. IVC: inferior vena cava; S: pacing stimulus; TA: tricuspid annulus.*

the CARTO. The present study showed that only monitoring of activation sequence of the lateral wall recorded by the DPC during PCS pacing led to the diagnostic errors in 11% of the patients.

## *Limitations of Activation Mapping Using DPC*

### *Residual Isthmus Conduction that Mimics Complete Isthmus Block*

One of the limitations of the activation mapping utilizing the DPC is the inability to detect the residual isthmus conduction that is slow enough to allow a wavefront propagating in an opposite direction to reach the ablation line earlier than the trans-isthmus conduction (here called *"concealed isthmus conduction"*) [3,4,7]. Theoretically, a very slow yet persistent isthmus conduction can be confined within the ablation line or a part of the isthmus distant from an area mapped by the DPC therefore be misdiagnosed, no matter how close to the ablation line the distal tip of the DPC was placed, or even if the DPC was positioned across the ablation line. Whether very slow isthmus conduction could be detected would depend on the spatial relationship between the location of the DPC and the conduction gap on the ablation line. As observed in two patients with *concealed isthmus conduction* in this study, the very slow isthmus conduction would not be detected if the DPC was placed at the isthmus near the TA and a conduction gap was located at the IVC edge of the isthmus. Among them, a simple rotation of the DPC to direct the DPC more posteriorly might have uncovered the incomplete CW isthmus block, although the transversal conduction across the RA posterior wall in the presence of complete isthmus block would not be excluded instantly (discussed later).

Several methods have been reported to distinguish the *concealed isthmus conduction* from the complete isthmus block [3]. One of the most frequently utilized methods is to map on the entire ablation line and examine whether a corridor of

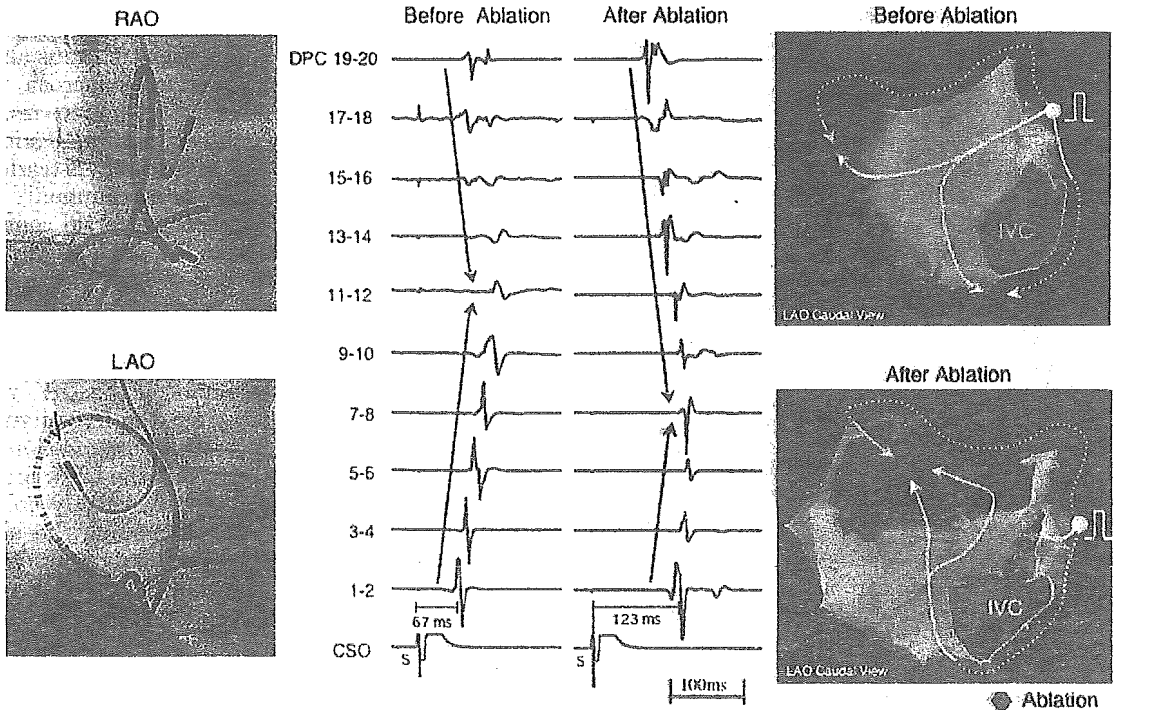


***Fig. 4.*** *The catheter position (left panel), the intracardiac recordings from the DPC and the CS catheter during proximal CS pacing with a cycle length of 500 ms before and after the ablation (middle panel), and the CARTO maps of the RA during proximal CS pacing before and after the isthmus ablation (right panel) in a patient with the collision pattern in the DPC recording in spite of complete isthmus block.* ***Left panel,*** *The distal dipole of the DPC was positioned near the TA just lateral to the ablation line.* ***Middle panel,*** *The collision site of the CW and CCW wavefronts shifted from DPC 11–12 (left, before ablation) to 7–8 (right, after ablation), but the collision pattern did not disappear after ablation. The time interval from the pacing stimulus to the atrial electrogram at DPC 1–2 prolonged after the isthmus ablation.* ***Right panel.*** *Before the isthmus ablation, the CW and CCW wavefronts collided at the lateral wall (upper). The remapping after the ablation demonstrated complete isthmus ablation (lower). However, an early wavefront from the posterior wall (shown by the red region) propagated around the IVC into the isthmus and collided with the CCW wavefront at the low lateral wall (shown by the purple region). CSO: ostium of coronary sinus; DPC: duodecapolar catheter; IVC: inferior vena cava; S: pacing stimulus.*

widely-split double potentials were recorded all along the ablation line during PCS or LLRA pacing [3]. At sites with a conduction gap, a fragmented potential could be recorded, as seen in two patients in our study. However, it was reported that clear-cut double potentials were not necessarily recorded on the ablation line despite the achievement of the complete isthmus block, and ambiguous electrograms such as triple or fragmented electrograms were recorded from the ablation line because of the multiple and broad linear ablation lesions or the presence of the dead-end pathways connected to the ipsilateral side to the pacing site [7]. Recently, Shah et al. [9] postulated a novel pacing method named "differential pacing" to overcome the above-mentioned limitations of the double potential criteria by comparing the intervals from the pacing stimulus to the terminal component of double or multiple potential recorded on the ablation line during the pacing from LLRA just lateral to the ablation line and more lateral to it. Although the positive predictive value of the differential pacing to diagnose the complete isthmus block was as high as 94% in their study, consistent results were not obtained intrapersonally in 50% of the patients with the persistent isthmus conduction, when the double potentials for the electrogram analyses were recorded at several sites on the ablation line in a single patient. Even with the differential pacing, depending on the spatial relationship between the locations of conduction gap and the double potential recording site on the ablation line, the possibility to misdiagnose the incomplete block as the complete block might not be completely excluded. In order to raise the diagnostic accuracy as much as possible, detailed mapping around the isthmus and all along the ablation line should be performed using above-mentioned methods concomitantly.

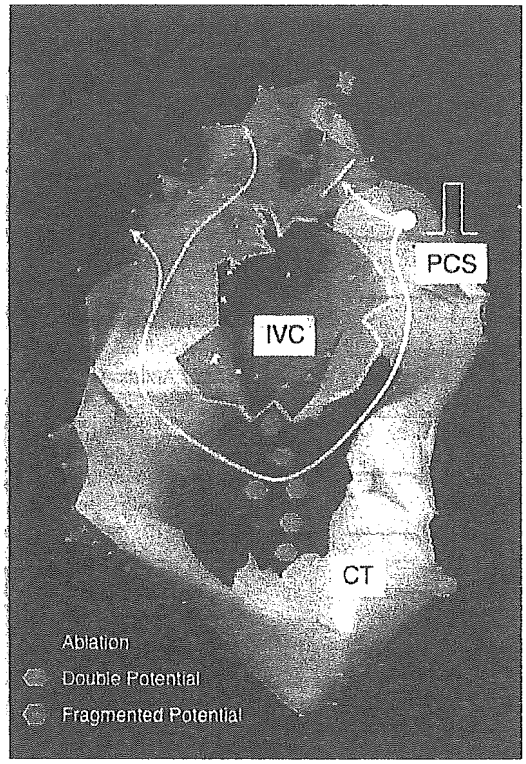


*Fig. 5. The CARTO remap during proximal CS pacing, viewed from the bottom, in the same patient as in Fig. 4. Mapping around the IVC orifice revealed the earlier wavefronts conducting transversally across the lower CT (red region). The double potentials (blue tags) were recorded at the middle part of the presumed site of the CT and the fragmented potentials (pink tags) were recorded at the lower part of the CT, suggesting the transversal conduction across the lower CT. CT: crista terminalis; IVC: inferior vena cava; PCS: proximal coronary sinus.*

### *Transversal Conduction Across CT that Mimics Incomplete Isthmus Block*

Another clinically important limitation of the activation mapping is the inability to differentiate the presence of the residual isthmus conduction from a situation where a wavefront that traverses across the posterior wall reaches the ablation line earlier than that traveling counter-clockwisely around the TA during CS pacing in the presence of the complete CW isthmus block (here called "*pseudo-conduction*") [5–7]. Although the CT was initially identified as the anatomical structure supporting the posterior transversal conduction block during AFL [10], several studies have shown that the transversal conduction block at the CT was mainly functional. Arenal et al. [6] reported in as much as 82% of patients with AFL, the transversal conduction across the CT was observed during the low rate pacing from the CS or the posterior wall. Scaglione et al. [9] reported that the *pseudo-conduction* was observed in 3 out of 12 patients (25%) with AFL who underwent isthmus ablation. Both the transversal conduction across the CT and/or the residual isthmus conduction can, therefore, lead to the incomplete isthmus conduction pattern in the DPC recording [5–7]. As transversal conduction across the CT occurs commonly [6] and the wavefront due to this transversal conduction comes from the posterior RA during PCS pacing after the isthmus ablation [5], the position of the DPC placement is expected to greatly influence the incidence of the *pseudo-conduction*. Although the DPC was positioned as close to the TA as possible in this study, the placement of the DPC to more posterior region away from the TA might have increased the incidence of the *pseudo-conduction* pattern in the recordings from the DPC. Similarly, to the results from our study, shortly split double potentials were recorded along the ablation line during PCS pacing among patients with the *pseudo-conduction* in the previous studies [5–7]. In our patients with collision pattern in the DPC recording, the presence of single or fragmented potentials on the ablation line predicted the residual isthmus conduction, whereas the presence of the shortly-split double potentials all along the ablation line predicted the *pseudo-conduction*. Although the double potentials on the ablation line do not always suggest the complete isthmus block [2], and there is no optimal cut-off value of the interpotential interval between the initial and terminal components of the double potential that can ensure the presence of the complete isthmus block, the presence of the double potential with any interpotential intervals all along the ablation line was considered as a good indicator of the complete isthmus block, regardless of the influence of the transversal CT conduction on the activation sequence of the DPC recording.

Despite the evidences that in most patients with AFL the CT has a transversal conduction property during low-rate CS pacing [6], it rarely influenced the peri-annular activation sequence and mimicked the persistent isthmus conduction in only 9% in this study. This observation suggests that the activation of the lateral wall, at least close to the TA, is in most cases independent of the transversal conduction state of the CT. The occurrence of the *pseudo-conduction* may depend on the relationship among the conduction velocity and the dimension around the TA and the IVC orifices.

### *Study Limitations*

Major limitation of the study is that there is already a significant body of literature that points out that the activation mapping as performed in this study is not enough to conclude that isthmus

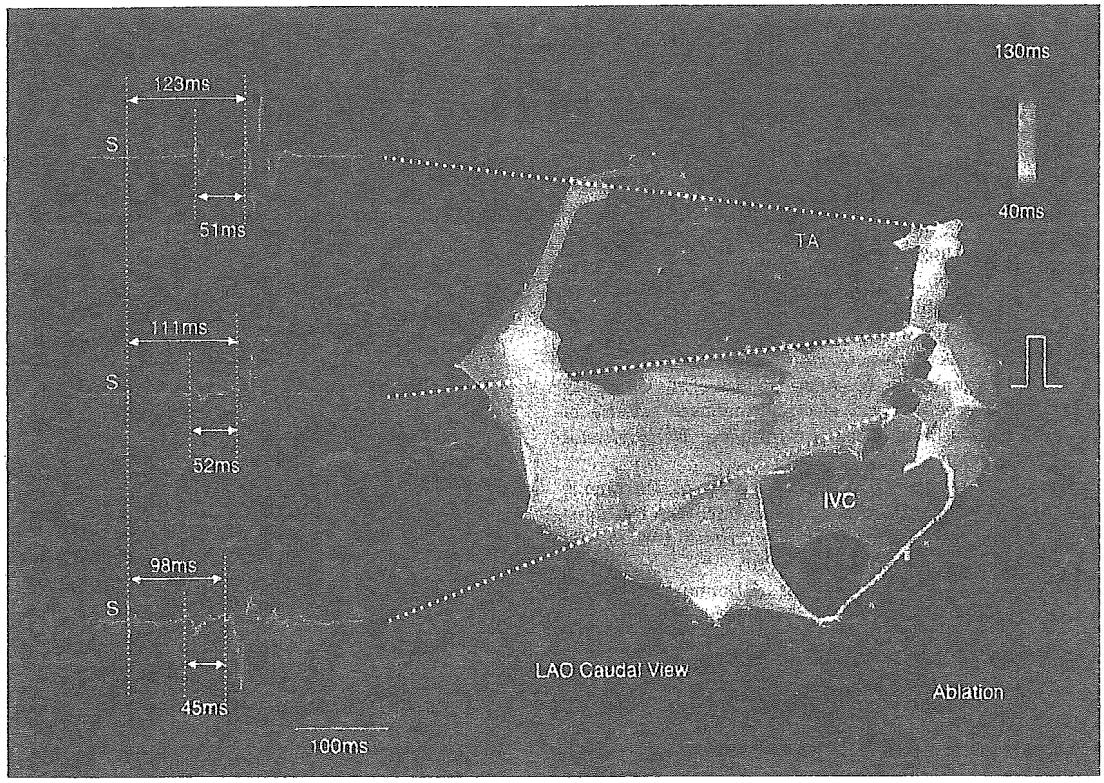


***Fig. 6.*** *A CARTO remap after the isthmus ablation during proximal CS pacing (right) and the bipolar electrograms recorded on the ablation line (left) in the same patient as in Fig. 4.* ***Right panel,*** *A wavefront from the posterior wall due to the transversal conduction across the CT pre-excited the lateral part of the isthmus earlier than the CCW wavefront around the TA and collided with the CCW wavefront at the lateral wall (purple region). The color bar indicates the activation time of each site, depicting the earliest activation site as red and the latest activation site as purple.* ***Left panel,*** *The shortly-split double potentials were recorded on the ablation line at the tricuspid annular, middle, and inferior vena caval parts, respectively. IVC: inferior vena cava; S: pacing stimulus; TA: tricuspid 4 annulus.*

block has been achieved. We did not systematically perform the differential pacing before the remapping using CARTO and did not evaluate the diagnostic ability of differential pacing that has been known to be superior to the activation mapping. Our intention of this study was to assess the actual frequency and the mechanisms of diagnostic failure of the activation mapping, which is the most simple and widespread method of evaluating the clockwise isthmus conduction, and not to recommend the universal use of electroanatomical mapping system for isthmus ablation and diagnosis of isthmus block. We did not perform the differential pacing before the CARTO remapping, therefore its diagnostic ability was not tested in this study. Furthermore, we only assessed CW isthmus conduction after ablation by activation mapping and the CCW isthmus block was verified only after CARTO remapping. In patients with sinus rhythm at the beginning of the electrophysiological study, a typical AFLs were not definitely ruled out as neither AFL induction nor entrainment pacing was not performed.

## *Conclusions*

After the TA-IVC isthmus ablation in patients with AFL, the atrial activation sequence recorded by the DPC positioned at the lateral RA along the TA mimicked the complete and incomplete CW isthmus block in 3 and 8% of all patients, despite the incomplete and complete block were demonstrated by the CARTO, respectively. These apparently complete and incomplete blocks were due to very slow isthmus conduction causing dissociated activation within the isthmus and the transversal conduction across the posterior wall causing preexcitation of the isthmus, respectively. It should be concluded that the mapping of the only lateral wall along the TA by the DPC during PCS pacing would not be sufficient for the diagnosis of

complete or incomplete CW isthmus block in some cases, therefore, it should be used in combination with other methods.

## References


1. Poty H, Saoudi N, Abdel Aziz A, Nair M, Letac B. Radiofrequency catheter ablation of type 1 atrial flutter. Prediction of late success by electrophysiological criteria. *Circulation* 1995;92:1389–1392.
2. Poty H, Saoudi N, Nair M, Anselme F, Letac B. Radiofrequency catheter ablation of atrial flutter. Further insights into the various types of isthmus block: Application to ablation during sinus rhythm. *Circulation* 1996;94:3204–3213.
3. Shah DC, Takahashi A, Jais P, Hocini M, Clementy J, Haissaguerre M. Local electrogram-based criteria of cavotricuspid isthmus block. *J Cardiovasc Electrophysiol* 1999;10:662–669.
4. Takahashi R, Iesaka Y, Takahashi A, Hiroe M, Marumo F. Clinical significance of residual slow cavotricuspid isthmus conduction after ablation of typical atrial flutter. *Pacing Clin Electrophysiol* 2000;23:1902–1907.
5. Scaglione M, Riccardi R, Calo L, Di Donna P, Lamberti F, Caponi D, Coda L, Gaita F. Typical atrial flutter ablation: Conduction across the posterior region of the inferior vena cava orifice may mimic unidirectional isthmus block. *J Cardiovasc Electrophysiol* 2000;11:387–395.
6. Arenal A, Almendral J, Alday JM, Villacastin J, Ormaetxe JM, Sande JL, Perez-Castellano N, Gonzalez S, Ortiz M, Delcan JL. Rate-dependent conduction block of the crista terminalis in patients with typical atrial flutter: Influence on evaluation of cavotricuspid isthmus conduction block. *Circulation* 1999;99:2771–2778.
7. Anselme F, Savoure A, Cribier A, Saoudi N. Catheter ablation of typical atrial flutter: A randomized comparison of 2 methods for determining complete bidirectional isthmus block. *Circulation* 2001;103:1434–1439.
8. Nakagawa H, Jackman WM. Use of a three-dimensional, nonfluoroscopic mapping system for catheter ablation of typical atrial flutter. *Pacing Clin Electrophysiol* 1998;21:1279–1286.
9. Shah D, Haissaguerre M, Takahashi A, Jais P, Hocini M, Clementy J. Differential pacing for distinguishing block from persistent conduction through an ablation line. *Circulation* 2000;102:1517–1522.
10. Olgin JE, Kalman JM, Fitzpatrick AP, Lesh MD. Role of right atrial endocardial structures as barriers to conduction during human type I atrial flutter. Activation and entrainment mapping guided by intracardiac echocardiography. *Circulation* 1995;92:1839–1848.

# Artificial Baroreflex

## Clinical Application of a Bionic Baroreflex System

Fumiyasu Yamasaki, MD; Takahiro Ushida, MD; Takeshi Yokoyama, DDS; Motonori Ando, PhD; Koichi Yamashita, MD; Takayuki Sato, MD

***Background***—We proposed a novel therapeutic strategy against central baroreflex failure: implementation of an artificial baroreflex system to automatically regulate sympathetic vasomotor tone, ie, a bionic baroreflex system (BBS), and we tested its efficacy in a model of sudden hypotension during surgery.

***Methods and Results***—The BBS consisted of a computer-controlled negative-feedback circuit that sensed arterial pressure (AP) and automatically computed the frequency (STM) of a pulse train required to stimulate sympathetic nerves via an epidural catheter placed at the level of the lower thoracic spinal cord. An operation rule was subsequently designed for the BBS using a feedback correction with proportional and integral gain factors. The transfer function from STM to AP was identified by a white noise system identification method in 12 sevoflurane-anesthetized patients undergoing orthopedic surgery involving the cervical vertebrae, and the feedback correction factors were determined with a numerical simulation to enable the BBS to quickly and stably attenuate an external disturbance on AP. The performance of the designed BBS was then examined in a model of orthostatic hypotension during knee joint surgery (n=21). Without the implementation of the BBS, a sudden deflation of a thigh tourniquet resulted in a 17±3 mm Hg decrease in AP within 10 seconds and a 25±2 mm Hg decrease in AP within 50 seconds. By contrast, during real-time execution of the BBS, the decrease in AP was 9±2 mm Hg at 10 seconds and 1±2 mm Hg at 50 seconds after the deflation.

***Conclusions***—These results suggest the feasibility of a BBS approach for central baroreflex failure. (***Circulation.* 2006; 113:634-639.**)

**Key Words:** baroreceptors ■ blood pressure ■ computers ■ electrical stimulation ■ nervous system, sympathetic

The arterial baroreflex acts to maintain cerebral perfusion by quickly attenuating the effect of an external disturbance, such as the assumption of an upright position, on arterial pressure (AP).[1–4] Therefore, functional restoration of dynamic properties of the arterial baroreflex is essential for the treatment of patients with various syndromes of baroreflex failure,[5] including Shy-Drager syndrome,[6–9] baroreceptor deafferentation,[10,11] and traumatic spinal cord injuries.[12,13] However, most commonly used interventions, including salt loading,[14,15] cardiac pacing,[16,17] and adrenergic agonists,[18,19] can neither restore nor reproduce the functioning of the native vasomotor center, and most affected patients remain bedridden.

### Clinical Perspective p 639

We recently developed a framework for identifying an operational rule of the vasomotor center and a prototype of a bionic baroreflex system (BBS) in rats.[20–22] The BBS consisted of a negative-feedback system controlled by a computer (ie, the artificial vasomotor center) that sensed AP and automatically computed the frequency of a pulse train required to stimulate sympathetic efferent nerves through a pair of wire electrodes placed in the celiac ganglion. Previous experimental work demonstrated that the BBS restored native baroreflex function in rats with central baroreflex failure; however, an applicable neural interface with quick and effective controllability of AP is required for application of this technology in the clinical setting. The goal of the present study was to determine the efficacy of a novel bionic technology for the intraoperative restoration of AP in the context of central baroreflex failure and to validate this technology in a clinical model of orthostatic hypotension.

## Methods

All studies were approved by the institutional review committee, and all subjects gave informed consent.

### Theoretical Considerations

As previously described,[20–22] the principle of the BBS is based on a negative-feedback mechanism (Figure 1). The instantaneous AP is measured by a pressure transducer connected to a computer that functions as a controller or artificial vasomotor center. Instead of the disabled native vasomotor center, the controller automatically exe-

Received September 8, 2005; revision received October 31, 2005; accepted November 21, 2005.

From the Departments of Cardiovascular Control (F.Y., M.A., T.S.), Clinical Laboratory (F.Y.), Orthopedic Surgery (T.U.), and Anesthesiology (T.Y., K.Y.), Kochi Medical School, Nankoku, Japan.

Correspondence to Fumiyasu Yamasaki, MD, Department of Clinical Laboratory, Kochi Medical School, Nankoku 783-8505, Japan. E-mail yamasakf@med.kochi-u.ac.jp



*Circulation* is available at http://www.circulationaha.org

DOI: 10.1161/CIRCULATIONAHA.105.587915